Functional Human Vascular Network Generated in Photocrosslinkable Gelatin Methacrylate Hydrogels

Ying-Chieh Chen, Ruei-Zeng Lin, Hao Qi, Yunzhi Yang, Hojae Bae, Juan M. Melero-Martin, and Ali Khademhosseini**

The generation of functional, 3D vascular networks is a fundamental prerequisite for the development of many future tissue engineering-based therapies. Current approaches in vascular network bioengineering are largely carried out using natural hydrogels as embedding scaffolds. However, most natural hydrogels present a poor mechanical stability and a suboptimal durability, which are critical limitations that hamper their widespread applicability. The search for improved hydrogels has become a priority in tissue engineering research. Here, the suitability of a photopolymerizable gelatin methacrylate (GelMA) hydrogel to support human progenitor cell-based formation of vascular networks is demonstrated. Using GelMA as the embedding scaffold, it is shown that 3D constructs containing human blood-derived endothelial colony-forming cells (ECFCs) and bone marrow-derived mesenchymal stem cells (MSCs) generate extensive capillary-like networks in vitro. These vascular structures contain distinct lumens that are formed by the fusion of ECFC intracellular vacuoles in a process of vascular morphogenesis. The process of vascular network formation is dependent on the presence of MSCs, which differentiate into perivascular cells occupying abluminal positions within the network. Importantly, it is shown that implantation of cell-laden GelMA hydrogels into immunodeficient mice results in a rapid formation of functional anastomoses between the bioengineered human vascular network and the mouse vasculature. Furthermore, it is shown that the degree of methacrylation of the GelMA can be used to modulate the cellular behavior and the extent of vascular network formation both in vitro and in vivo. These data suggest that GelMA hydrogels can be used for biomedical applications that require the formation of microvascular networks, including the development of complex engineered tissues.

1. Introduction

The success of tissue engineering as a feasible approach in regenerative medicine relies largely on our ability to generate 3D vascular networks that guarantee adequate oxygenation, nutrient delivery and removal of waste products.[1–3] These vascular networks would need to be developed within clinically suitable biomaterials and in a timely manner to ensure rapid reconnection with the host vasculature and to avoid loss of cellular viability. Strategies to ensure appropriate vascularization have included the delivery of angiogenic molecules as a means of promoting the ingrowth of pre-existing host microvessels.[4–6] However, the ingrowth of angiogenic sprouts is not sufficient to achieve rapid and complete vascularization of thick tissue-engineered constructs.[3,7] More recently, cell-based approaches that exploit the inherent blood vessel-forming ability of endothelial cells (ECs) have also been proposed.[8–13] Among these strategies, the use of blood-derived endothelial colony-forming cells (ECFCs) and mesenchymal stem cells (MSCs) is particularly appealing because they both can be obtained by non-invasive means and can

Dr. Y.-C. Chen, Dr. H. Qi, Dr. H. Bae, Prof. A. Khademhosseini
Department of Medicine
Center for Biomedical Engineering
Brigham and Women's Hospital
Harvard Medical School, Boston, MA 02115, USA
E-mail: alik@rics.bwh.harvard.edu
Dr. Y.-C. Chen, Dr. H. Qi, Prof. A. Khademhosseini
Wyss Institute for Biologically Inspired Engineering
Harvard Medical School
Boston, MA 02155, USA
Dr. Y.-C. Chen
Department of Applied Science
National Hsinchu University of Education
Hsinchu 300, Taiwan
Dr. R.-Z. Lin, Prof. J. M. Melero-Martin
Department of Cardiac Surgery
Children's Hospital Boston
Boston, MA 02115, USA
E-mail: Juan.MeleroMartin@childrens.harvard.edu
Dr. R.-Z. Lin, Prof. J. M. Melero-Martin
Department of Surgery
Harvard Medical School
Boston, MA 02115, USA
Prof. Y. Yang
Department of Orthopedic Surgery
Stanford University
300 Pasteur Drive, Edwards, R155, Stanford, CA 94305, USA
Prof. Y. Yang
Houston Biomaterials Research Center
Department of Restorative Dentistry and Biomaterials
University of Texas Health Science Center at Houston
Houston, TX 77030, USA
Dr. H. Bae, Prof. A. Khademhosseini
Harvard-MIT Division of Health Sciences and Technology
Massachusetts Institute of Technology
Cambridge, MA 02139, USA

DOI: 10.1002/adfm.201101662

be extensively expanded in vitro.[10,11,14] Studies have shown that combining both human ECFCs and MSCs results in the formation of robust functional vascular networks in murine models of human cell transplantation.[11–13] These vascular networks are formed within the first week after transplantation and they remain stable and functional thereafter.[11] Importantly, both cell types have been proven to be essential in generating a functional vasculature, with ECFCs restricted to the luminal aspect of the vessels and MSCs adjacent to the lumens as perivascular cells.[11]

A critical aspect for the development of clinical cell-based strategies is the use of suitable biomaterials.[15] In the most current models of vasculature formation, cells are embedded in either Matrigel or other natural collagen-based hydrogels, all of which are favorable microenvironments for vascular morphogenesis.[16,17] However, some of the properties of these materials are not ideal for tissue engineering applications: Matrigel is derived from murine tumors and is therefore not suitable for clinical use;[18] collagen-based gels also present limitations, such as poor mechanical stability and suboptimal durability.[19,20] Furthermore, the clinical use of animal-derived extracellular matrix (ECM) proteins is often restricted due to immunogenic concerns.[21,22] Accordingly, improving the properties of naturally occurring ECMs has become a crucial priority in tissue engineering research.[23] This can be achieved by the chemical functionalization of proteins, an approach that was proposed precisely to improve the usability of biomaterials.[24,25] One recent example is the development of gelatin methacrylate (GelMA) hydrogels.[26] GelMA is synthesized by adding methacrylate groups to the amine-containing side-groups of gelatin, which becomes a photocrosslinkable hydrogel.[26] As a result, GelMA hydrogels carry advantages that are representative characters of both natural and synthetic biomaterials. In particular, GelMA contains gelatin as its backbone, which provides cell-responsive characteristics such as the provision of appropriate cell adhesion sites and proteolytic degradability.[20,26,27] Also, gelatin can be derived inexpensively from a variety of sources.[27] Moreover, we have shown that methacrylation and photocrosslinking provide tunable mechanical and chemical properties, including the ability to create 3D microarchitectures.[26,28,29]

Here we propose the use of photocrosslinkable GelMA hydrogel as a permissive biomaterial for the formation of functional vascular networks. We have carried out preclinical studies and demonstrate that extensive human ECFC-lined vascular networks can be generated in GelMA and that these networks can form functional anastomoses with existing vasculature when transplanted into immunodeficient mice.

2. Results

2.1. Synthesis and Characterization of GelMA Hydrogels

Three different GelMA hydrogels were synthesized using 1M, 5M, and 10M methacrylic anhydrate. The actual percentages of the functionalized methacrylation groups were determined by measuring the extent of free amine group substitution using ^{1}H-NMR spectroscopy. The degree of methacrylation (defined as the ratio of functionalized to original amino groups) corresponded to 49.8%, 63.8% and 73.2% for the 1M, 5M and 10M GelMA hydrogels, respectively. The mechanical properties of each synthesized GelMA hydrogel were evaluated using an unconfined compression test (**Figure 1**a). As expected, we found that the compressive modulus of the GelMA increased with its methacrylation degree: 2.0 ± 0.18 kPa (1M), 3.2 ± 0.18 kPa (5M) and 4.5 ± 0.33 kPa (10M) (Figure 1a). The degradation of the GelMA hydrogels was quantified in collagenase solution by monitoring the percentage of hydrogel residual mass as a function of time (Figure 1b). The degradation rate decreased with the methacrylation degree of the GelMA; the 1 M GelMA hydrogels underwent complete degradation within 6 h, whereas the 10M GelMA hydrogels lasted for 15 h. The microstructures

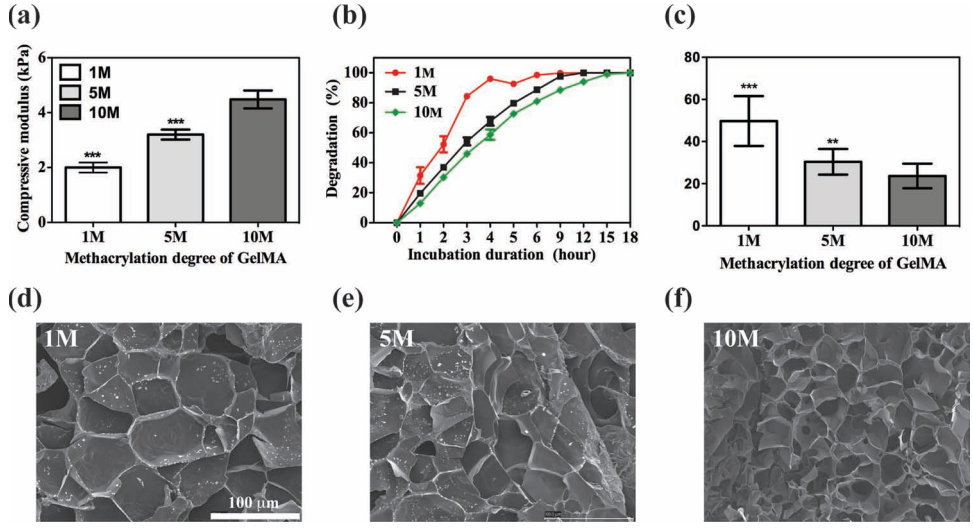

Figure 1. a–f) Characterization of GelMA hydrogels with different methacrylation degrees: compressive modulus (a); degradation profiles upon incubation with collagenase (b); average pore size (c); SEM images (d–f). The data are presented as the mean ± the standard deviation (SD). **: $p < 0.01$, ***: $p < 0.001$, compared with the 10M GelMA.

of the GelMA hydrogels were observed by field-emission scanning electron microscopy (FE-SEM) (Figure 1 d–f). The SEM images revealed uniform porous microstructures throughout all the samples. The average size of interconnected pores decreased with higher degrees of methacrylation from 49.7 ± 11.8 μm and 30.13 ± 6.12 μm to 23.6 ± 5.85 μm in the 1M, 5M, and 10M GelMA hydrogels, respectively (Figure 1c). Collectively, the degree of methacrylation was found to affect the physical and mechanical properties of the synthesized GelMA hydrogels, with higher methacrylation resulting in stiffer and more durable hydrogels, with smaller pore sizes.

2.2. Monoculture of ECFCs and MSCs in GelMA Hydrogels

To assess the effect of the methacrylation degree on cell proliferation, ECFCs labeled with DsRed, a red-fluorescence protein, and MSCs labeled with 5-chloromethylfluorescein diacetate (CMFDA), a green fluorescence Celltracker, were encapsulated in GelMA hydrogels, independently, and cultured in endothelial growth medium 2 (EGM-2). Previous studies have shown that a dose of UV irradiation does not compromise the cell viability.[26,30] Cells were harvested from each hydrogel after 2, 4 and 6 d of culture and the number of cells retrieved was normalized to the original seeding cell number (**Figure 2**a–b). For both the ECFC and the MSC monocultures, the cell numbers decreased with the methacrylation degree at any given time point (Figure 2a–b). Regardless of the methacrylation degree used, there was no proliferation of ECFCs over time (Figure 2a); instead, cell survival was progressively compromised by time in culture, and was worse with a higher methacrylation degree. Qualitative images of intact hydrogels showed that the DsRed-ECFCs remained sparse and maintained round morphologies after 6 d in GelMA monoculture, indicating an inability to form capillary network structures (Figure 2c–e). On the other hand, MSCs were able to proliferate in the GelMA hydrogels, although the proliferation rate decreased with higher methacrylation degree (Figure 2b). CMFDA-labeled MSCs were able to spread in all of the GelMA hydrogels used, although the interconnected cellular network that formed was less extensive as the methacrylation degree increased (Figure 2f–h).

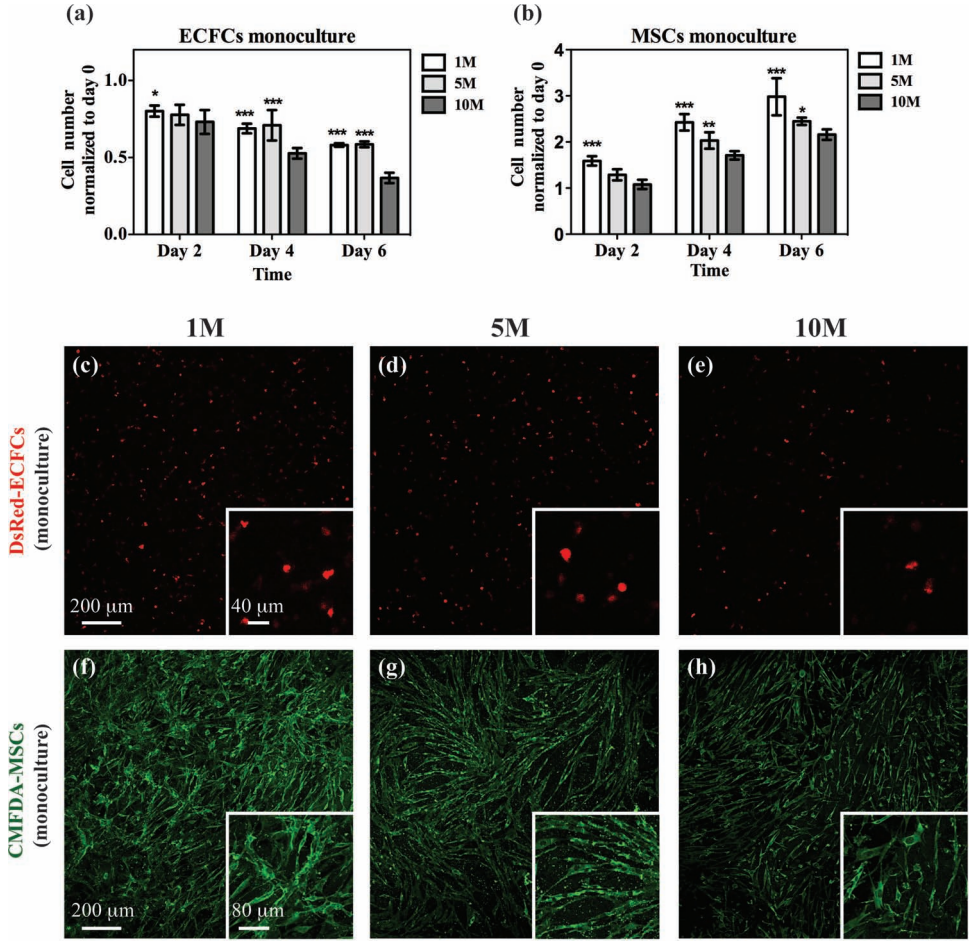

Figure 2. Monocultures of vascular cells embedded in GelMA. a,b) Monocultures containing either ECFCs (a) or MSCs (b) were evaluated for cell number at 2, 4 and 6 d using GelMA hydrogels with different methacrylation degrees. c–h) Representative confocal microscopy images of embedded DsRed-ECFCs (c–e) and CMFDA-labeled MSCs (f–h) after day 6 in monoculture for each methacrylation degree. The insets show images taken at higher magnification. The data are presented as the mean ± SD. *: $p < 0.1$, **: $p < 0.01$, ***: $p < 0.001$, compared with the 10M GelMA.

2.3. Co-Cultures of ECFCs and MSCs in GelMA Hydrogels

Next, we evaluated the ability of ECFCs and MSCs to proliferate, spread and organize when co-cultured (1:1 ratio) inside GelMA hydrogels with different methacrylation degrees (**Figure 3**). Similarly to monoculture, we found that both the ECFC and the MSC numbers decreased with increased methacrylation degree at any given time point (Figure 3a,b). However, we observed important differences between the monocultures and the co-cultures. First, the overall survival of ECFCs was increased by the presence of MSCs, although their survival was still compromised by higher methacrylation degrees. More importantly, the presence of MSCs induced the ECFCs to assemble into capillary-like networks (Figure 3c–e). These ECFC-networks were well established in the 1M GelMA, with the majority of ECFCs forming cord-like structures (Figure 3c). However, this network-forming ability was hampered with increasing methacrylation degree, as illustrated by the presence of non-aligned ECFCs in the 10M GelMA hydrogels (Figure 3e). Second, the presence of ECFCs impaired MSC proliferation (Figure 3b) and diminished the extent of MSC spreading that was prevalent in the monocultures (Figure 3f–h). This reduced MSC proliferation was confirmed by expression of Ki67. In monoculture, the percentage of Ki67-positive proliferative MSCs was 6.68% ± 3.9% at 6 d in the 1M GelMA, while in co-culture this percentage was drastically decreased to 0.83% ± 1% (Figure S1, Supporting Information). Collectively, coculture of ECFCs and MSCs in GelMA was found to be critical for both the survival of the ECFCs and the formation of ECFC-lined capillary-like networks. The GelMA was found to be a permissive biomaterial for capillary network formation, although an increased methacrylation degree progressively hampered this process.

2.4. In Vitro Capillary-Like Network Characterization

The extent of capillary-like network formation was quantified in the co-cultured hydrogels using confocal microscopy (**Figure 4**). Quantification of the DsRed-ECFC-lined structures was carried

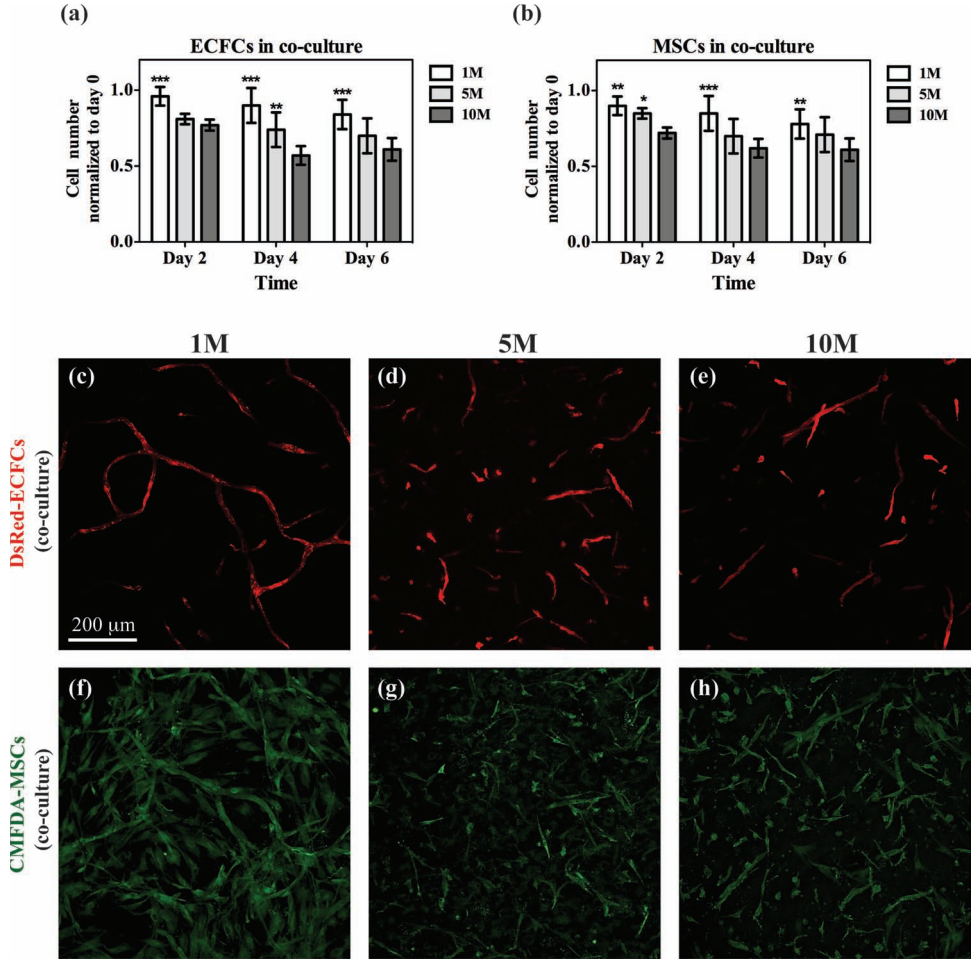

Figure 3. Co-culture of vascular cells in GelMA. Constructs containing both DsRed-ECFCs and CMFDA-labeled MSCs were cultured for 2, 4 and 6 d using GelMA hydrogels with different methacrylation degrees. a,b) Numbers of DsRed-ECFCs (a) and CMFDA-MSCs (b) were separately counted at each time point under a fluorescence microscope. c–h) Representative confocal microscopy images of DsRed-ECFCs (c–e) and CMFDA-MSCs (f–h) after day 6 in co-culture for each methacrylation degree. The data are presented as the mean ± SD. *: $p < 0.1$, **: $p < 0.01$, ***: $p < 0.001$, compared with the 10M GelMA.

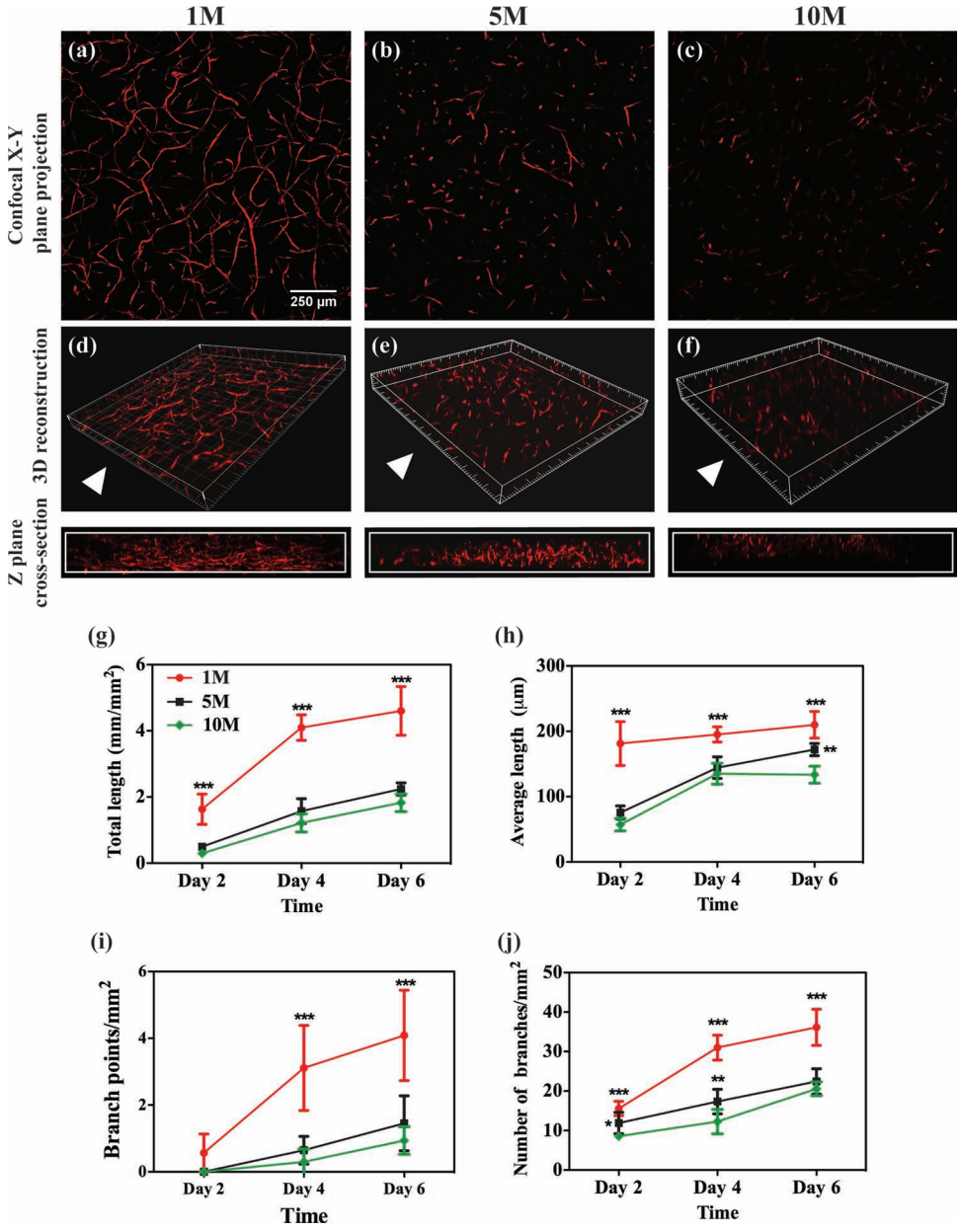

Figure 4. Extent of capillary-like network formation. Constructs containing both DsRed-ECFCs and CMFDA-labeled MSCs were cultured in the GelMA hydrogels with different methacrylation degrees. The DsRed-ECFCs were imaged in whole-mount constructs using confocal microscopy at day 6. a–c) Representative 2D projections ($x-y$ plane) of images collected along the z -axis of the constructs. d–f) Representative 3D reconstruction of constructs from confocal microscopy images: z -plane cross-sections covering a thickness of 400 μm are in the direction of the white arrows. A representative video of a rotating 3D reconstruction of the confocal images showing interconnected vascular networks is available (Video 1, Supporting Information) g–j) Quantitative analysis of the extent of capillary-like network formation after 2, 4 and 6 d in vitro was carried out by measuring total capillary-like length per unit of area (g), the average length of capillaries (h), the number of branch points per unit of area (i) and the number of branches per unit of area (j). The data are presented as the mean ± SD. *: $p < 0.1$, **: $p < 0.01$, ***: $p < 0.001$, compared with the 10M GelMA.

out in z-stack projected images generated from the 1M, 5M, and 10M GelMA constructs (Figure 4a–c). These images clearly reveal that the extent of network formation was hampered by increased methacrylation; the GelMA with the lowest methacrylation degree (1 M) consistently generated more robust, 3D, interconnected vascular networks than the 5M and 10M GelMA hydrogels (Figure 4d –f and Video 1, Supporting Information), with significantly higher total network length (Figure 4g), average branch length (Figure 4h), number of branch points (Figure 4i) and number of branches (Figure 4j) at every time point analyzed. Additional network visualization was carried out using 3D-reconstructed images from each cell-laden hydrogel

(Figure 4d–f), showing differential cellular interconnectivity with different methacrylation degrees. These differences were uniformly observed throughout the entire thickness of the hydrogel constructs. Capillary-like networks in 1M GelMA were already visible at day 2 (Figure 4g–j), with maximum extension rate between days 2 and 4. Total network extension occurred by progressive formation of new branches (Figure 4i–j), as opposed to the extension of existing branches, which remained at a fairly constant length (Figure 4h and Video 1, Supporting Information). In contrast, in highly methacrylated GelMA, networks were formed by significantly fewer numbers of branches, the extension of which were responsible for the overall growth of the network over time.

The presence of MSCs was crucial for the formation of ECFC-lined capillary networks. α-Smooth muscle actin (αSMA)-expressing MSCs were visualized both in proximity and adjacent to the capillary structures, suggesting an ongoing process of perivascular coverage of capillaries (**Figure 5**). At 6 d of coculture, the perivascular coverage and MSC-wrapped capillaries were more robust in the 1M GelMA (Figure 5a and Video 2, Supporting Information) than they were in the 10M GelMA (Figure 5c), indicating that the methacrylation degree affected not only the number of ECFC branches, but also the attraction of MSCs toward these capillaries. Moreover, the methacrylation degree also affected the ability of the MSCs to differentiate into smooth muscle/pericytes (Figure 5b,d), as indicated by the expression of the smooth muscle myosin heavy chains (sm-MHCs) found in the 1M GelMA (Figure 5b) but not in the 10M hydrogel (Figure 5d). Taken together, these results indicate that the GelMA permitted close association of the MSCs with the ECFC-lined capillary-like structures and differentiation of MSCs into perivascular cells. The extent of each of these processes was affected by the methacrylation degree of the GelMA.

2.5. Formation of ECFC-Lined Lumens by the Fusion of Intracellular Vacuoles

A critical aspect of vascular network formation is the appearance of true EC-lined lumens.[31] The presence of DsRed-ECFC-lined lumens was investigated by a confocal microscopy examination of whole-mounted, cell-laden 1M GelMA hydrogels (**Figure 6**). Analyses of the constructs at 3, 6 and 10 d of culture revealed a progressive process of lumen morphogenesis (Figure 6 and Figure S2, Supporting Information). This process involved an initial accumulation of ECFC-specific intracellular vacuoles at day 3 (Figure 6a), which were intracellularly arranged into rows and were present in the majority of the ECFC-lined capillary structures (Figure S2, Supporting Information). Importantly, the surface of these vacuoles expressed CD31, a surface cellular

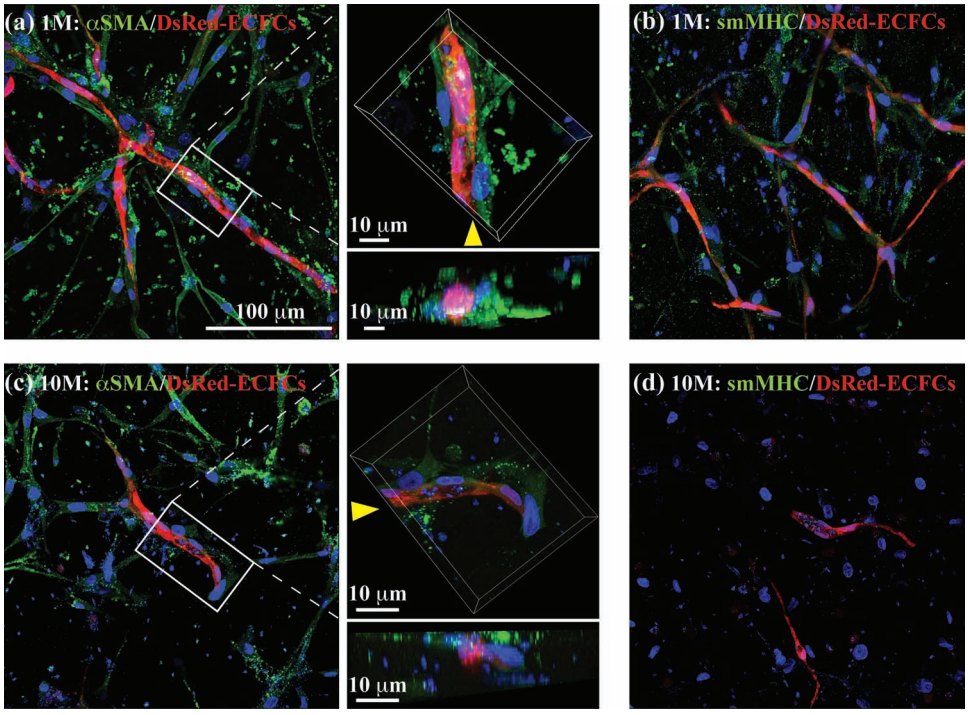

Figure 5. Stabilization of the ECFC-lined capillaries by perivascular cells. Constructs containing both DsRed-ECFCs and MSCs were cultured for 7 d in GelMA hydrogels with different methacrylation degrees. The ability of the MSCs to differentiate into perivascular cells was analyzed by confocal microscopy after immunoflourescence staining with antibodies against smooth muscle markers. a,c) Representative confocal images showing the spatial distribution of the DsRed-ECFC-lined capillaries surrounded by αSMA-expressing MSCs. Higher magnification images depicting details of a capillary (top) and a cross-section image taken in the direction of the white arrows (bottom) are shown to the right of the these images in panels (a) and (c). b,d) Representative confocal images showing the spatial distribution of both DsRed-ECFC-lined capillaries surrounded by sm-MHC-expressing MSCs. A representative video of a rotating 3D reconstruction of confocal images showing MSC-wrapped capillaries is available (Video 2, Supporting Information).

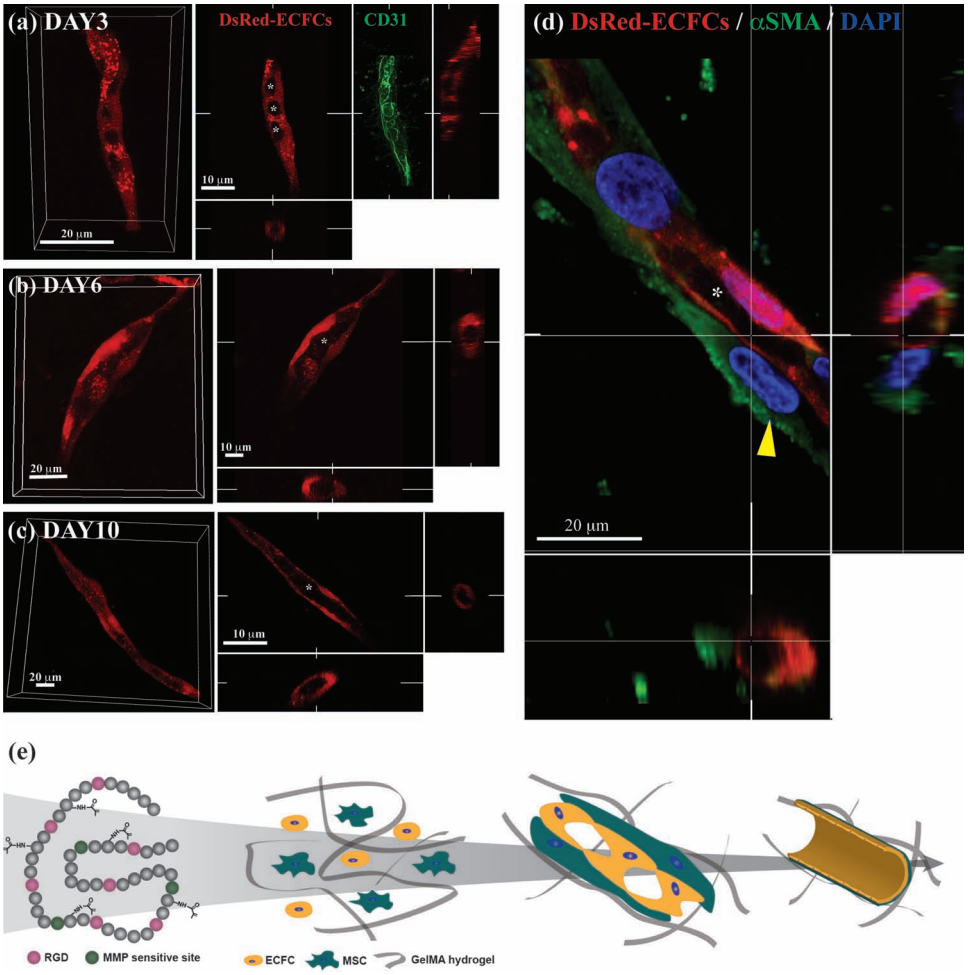

Figure 6. Formation of ECFC-lined lumens by fusion of intracellular vacuoles. Constructs containing both DsRed-ECFCs and MSCs were cultured for 7 d using 1M GelMA hydrogels. The presence of DsRed-ECFC-lined lumens was investigated by a confocal microscopy examination of whole-mounted constructs. Analyses of the constructs at 3, 6 and 10 d of culture reveal a progressive process of lumen morphogenesis. a) Initial accumulation of ECFC-specific intracellular vacuoles (asterisks) at day 3; the vacuoles were intracellularly arranged into rows and were present in the majority of the ECFC-lined capillary structures. The surface of these vacuoles were stained positive for human CD31. b) By day 6, larger vacuoles coalesced forming large, intracellular luminal structures. c) At day 10, hollow ECFC-lined lumens were identified unequivocally and uniformly distributed in discrete locations within the capillary-like structures. d) Lumens were lined exclusively by ECFCs and were surrounded by αSMA-expressing MSCs (yellow arrowhead). e) Schematic diagram depicting the steps of endothelial lumen formation in GelMA.

marker of ECs (Figure 6a). By day 6, some of the larger vacuoles had coalesced, forming large, intracellular luminal structures (Figure 6b). At day 10, hollow ECFC-lined lumens were unequivocally identified and uniformly distributed in discrete locations within the capillary-like structures (Figure 6c). These lumens were exclusively lined by ECFCs and were surrounded by αSMA-expressing MSCs (Figure 6d), presumably providing further luminal stabilization. These findings indicate that the 1M GelMA hydrogels offer a permissive environment for cell-mediated formation of lumen-containing capillaries network in vitro. The scheme shown in Figure 6e is based on our confocal immunofluorescence staining data and depicts the distinct steps of lumen formation. Notably, the mechanism described here is in line with the cord-hollowing mode, which implies that a lumen is created de novo in the intercellular space between polarizing cells within a cylindrical cord.

2.6. In Vivo Biocompatibility and Biodegradation of the GelMA Hydrogels

The biocompatibility and biodegradation of the GelMA hydrogels were evaluated in vivo after subcutaneous implantation into mice (**Figure 7**). Collagen-type 1 gel served as a control. A macroscopic view of the explanted hydrogels revealed different degradations with time and methacrylation degree (Figure 7a). The degradation was quantified by measuring the loss of volume (Figure 7b) and weight (Figure 7c) over time. The 1M GelMA hydrogels were partially degraded at day 7 and were completely resorbed at 28 d (96.14% volume loss and 96.55% weight loss). In contrast, the 10M GelMA hydrogels showed a slower degradation rate: 31.51% volume loss and 32.17% weight loss at day 7 and 35.84% volume loss and 52.25% weight loss at day 28. As expected, the control collagen gel degraded rapidly, with 95.4%

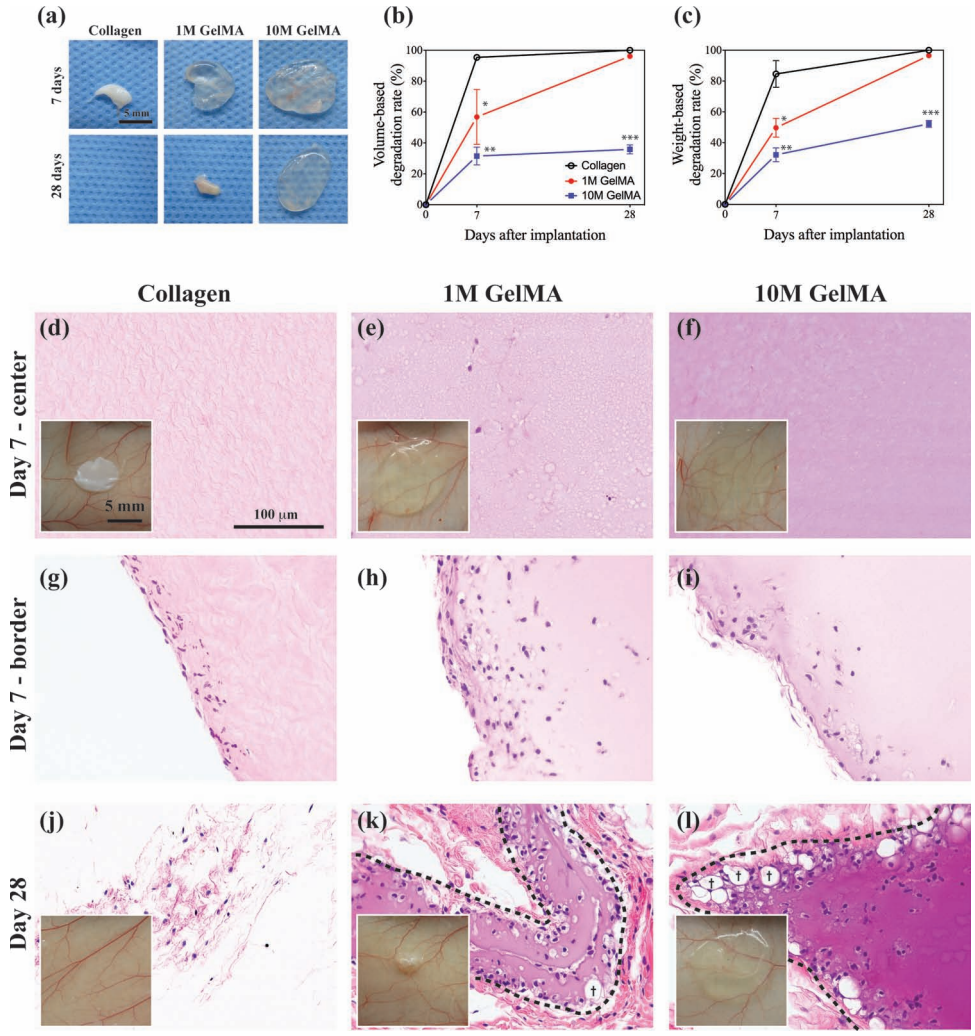

Figure 7. Evaluation of GelMA hydrogels in vivo. GelMA hydrogels with 1M and 10M methacrylation degrees and containing no cells were surgically implanted into the subcutaneous space on the backs of 6-week old nude mice. Rat-tail type-1-collagen gel served as a control. a) Macroscopic views of explanted gels after 7 and 28 d. b,c) In vivo gel degradation profiles based on volume (b) and weight (c) loss: $n = 3$ per gel type and time point. The data are presented as the mean ± SD. *: $p < 0.1$, **: $p < 0.01$, ***: $p < 0.001$, compared with collagen. d–l) Representative images of hematoxylin/eosin (H&E)-stained sections from collagen and the 1M and 10M GelMA implants, harvested at day 7 (d–i) and day 28 (j–l). The insets show representative photographs taken at the time of harvesting and depict the integration of implants with murine subcutaneous tissue at the site of implantation. The dashed lines delineate the implant border at day 28. "†" indicates adipocytes.

volume loss after day 7. Collectively, the in vivo biodegradation rates correlated with those obtained in vitro by collagenase degradation (Figure 1b), and decreased with increasing GelMA methacrylation degree.

The GelMA hydrogels did not evoke noticeable host inflammatory responses. Macroscopic views of the hydrogels at the implantation sites showed no evidence of inflammation in the surrounding subcutaneous tissue (Figure 7d–f, insets). Also, histological examinations at day 7 and day 28, of both the 1M and the 10M GelMA hydrogels, revealed a minimal infiltration of the murine cells, mainly being restricted to the hydrogel borders (Figure 7 d–i and Figure S3–S5, Supporting Information). Those host cells that did infiltrate appear to be mononuclear cells (e.g., monocytes/macrophages), as evidenced by their nuclear and cellular morphology. No foreign-body giant cells were found in any of the hydrogels evaluated. Ingrowth of murine blood vessels was observed only in few locations near the borders of both the 1M and 10M GelMA hydrogels at day 7 (Figure S3–S5, Supporting Information), indicating material compatibility with angiogenesis. The lack of an inflammatory response was corroborated by hematological analyses carried out in blood samples obtained from implant-bearing mice at different time intervals (**Figure S6**, Supporting Information). Shortly after surgical implantation, there were no significant differences between shamed-operated and implant-bearing mice: the total white blood cell number (WBC) and concentration of individual leukocytic subpopulations experienced a mild initial increase (day 3), returned to presurgery levels by day 7 and maintained these basal values afterwards (Figure S6, Supporting Information). Beyond day 3 though, and in addition to our hematological analyses,

we carefully examined all of our histologies from the hydrogel explants after 7 d (Figure 7d–i) and 28 d (Figure 7j–l) in vivo, and we did not observe the accumulation of polymorphonuclear cells, or any obvious presence of inflammatory cells in general. These results demonstrate the low immunogenicity of GelMA, independent of the methacrylation degree. At 28 d, the collagen implants were completely degraded in vivo (Figure 7a). Examination of the skin at the implantation site revealed normal subcutaneous tissue but no sign of the collagen implants (Figure 7j). Meanwhile, the GelMA constructs were still present at the implantation site after 28 d in vivo (Figure 7k,l).

2.7. In Vivo Formation of Human Vascular Networks

To determine whether the GelMA hydrogels could support the formation of vascular networks in vivo, we surgically implanted cell-laden hydrogels into immunodeficient mice (**Figure 8**). All of the implants were UV-crosslinked prior to implantation and consisted of 200 µL of hydrogel seeded with 5×10^5 ECFCs and 5×10^5 MSCs (Figure 8a). Collagen-type 1 gels served as a permissive biomaterial control. After 7 d, the constructs were explanted (Figure 8b–d insets) and examined for the presence of vascular structures. Histological examination carried out by hematoxylin/eosin (H&E) staining revealed that the extent of vascular network formation was different between the 1M and 10M GelMA constructs (Figure 8b–d). In the 1M GelMA, numerous blood vessels containing erythrocytes (yellow arrowheads; Figure 8c) were uniformly distributed throughout the explants. In contrast, there were fewer perfused blood vessels in the 10M GelMA, and those microvessels were mainly restricted to the periphery of the constructs (Figure 8d). The microvessels were stained positive for human CD31 (red arrowheads; Figure 8e–j and Figure S7–S9, Supporting Information), confirming the lumens were lined with implanted human ECFC cells. Infiltrated murine blood vessels were identified by negative hCD31 expression (green arrowheads; Figure 8e–g). A close examination of the human microvessels demonstrated they contained murine erythrocytes (Figure 8h–j), indicating that functional anastomoses with an existing murine vasculature had occurred. This result is important because it demonstrates that the formation of microvascular vessels within the GelMA hydrogels was carried out by the implanted cells and it was not just due to host blood vessel invasion. The distribution of human–specific microvessels was also different between the 1M and 10M GelMA constructs, with a higher number of hCD31-positive vessels in 1M GelMA. Also, the distribution of perfused and non-perfused vessels was non-uniform; in the 1M GelMA, perfused hCD31-positive vessels were distributed throughout the whole implant, but they were more prevalent in the proximity of host tissues (Figure S8, Supporting Information). Meanwhile, non-perfused human-ECFC-lined capillary-like structures were mainly observed in the center of implants, suggesting an ongoing process of connection between the human preformed capillaries and the mouse perfused vessels coming from the surrounding host tissues. In contrast, perfused human vessels in the 10M GelMA were highly restricted to the borders, and the central areas of these constructs were

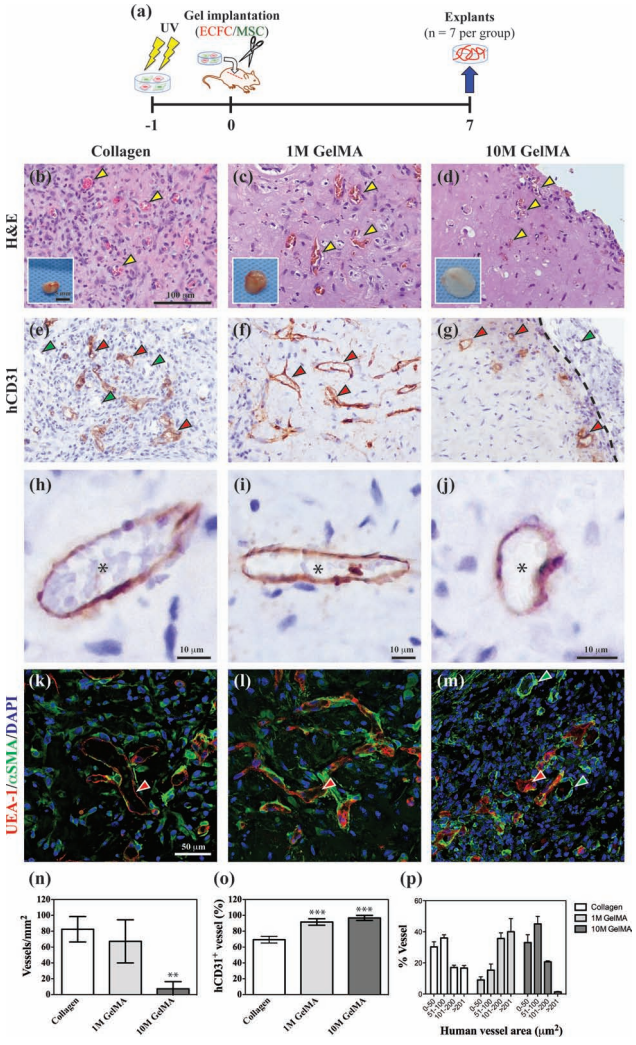

Figure 8. In vivo formation of functional vascular networks. a) Schematic diagram: the 1M and 10M GelMA hydrogels containing both ECFCs and MSCs were incubated in vitro for 24 h and surgically implanted into the subcutaneous space on the backs of 6-week old nude mice ($n = 7$ per gel type). Rat-tail type-1-collagen gel served as a control. The implants were retrieved after 7 d in vivo. b–d) Representative images of H&E-stained sections from collagen and the 1M and 10M GelMA explants, revealing the presence of numerous blood vessels containing murine erythrocytes (yellow arrowheads). Macroscopic views of the explants are depicted in the insets. e–g) Immunohistochemistry showed that the engineered microvessels were stained positive for human CD31 (red arrowheads), while the murine capillaries (green arrowheads) were not. h–j) Images at higher magnification showing a single human-CD31-expressing vessel (asterisks) carrying murine erythrocytes. k–m) Representative images of fluorescently stained sections using rhodamine-conjugated UEA-1 lectin (to mark human-ECFC-lined vessels) and fluorescein isothiocyanate (FITC)-conjugated anti-αSMA antibodies (to mark perivascular cells; red arrowheads). The UEA-1 lectin did not bind to the murine vessels (green arrowheads). The nuclei were stained with 4',6-diamidino-2-phenylindole (DAPI). n–p) The extent of the vascular-network formation was quantified by measuring the microvessel density (n), the percentage of human-CD31-expressing blood vessels (o), and the size distribution of the luminal cross-sectional area (p). The data are presented as the mean ± SD. **: $p < 0.01$, ***: $p < 0.001$, compared with the collagen implants.

populated by scattered hCD31-positive ECFCs that had failed to organize into capillary-like structures (Figure S9, Supporting Information). The human nature of the microvessels was also corroborated by specific binding of *Ulex europaeus agglutinin* (UEA)-1 (Figure 8k–m), a lectin that does not bind to murine endothelium (Figure S10, Supporting Information). Also, the large majority of human microvessels at day 7 was completely covered by αSMA-positive perivascular cells (Figure 8 k–m), a clear sign of vessel maturation.[32]

Quantification of the microvessel density revealed statistically significant differences between the 1M GelMA (58.34 ± 32.70 vessels mm^{-2}) and the 10M GelMA (7.20 ± 9.15 vessels mm^{-2}) (Figure 8n). Also, there were no significant differences between the 1M GelMA and the collagen constructs (82.49 ± 12.04 vessels mm^{-2}); moreover, as expected, the collagen gels underwent a significant contraction by day 7 (Figure 7), which inevitably resulted in an increased number of microvessels counted per unit of area. The percentage of vessels that were hCD31-positive was similar in the two GelMA constructs (in both, over 90%); this was significantly higher than in the collagen implants, in which more than 30% of the vessels were murine (Figure 8o). Finally, the degree of methacrylation also affected the luminal size of the blood vessels (Figure 8p), with larger lumens observed in the 1M GelMA than in the 10M GelMA. Collectively, these results prove that ECFCs are able to form extensive vascular networks in GelMA hydrogels and that these networks make functional connections with the mouse vascular system. These results also indicate that the degree of methacrylation can be used to tune both the vascular density and the average size of the vascular lumens achieved.

3. Discussion

The generation of functional 3D vascular networks is a long-pursued goal in tissue engineering and a fundamental prerequisite for mimicking the functionality and complexity of native tissues.[2,3,33] It has been long proposed that engineering a vascular bed can be carried out by a strategic combination of vascular cells.[10–13] In recent years, multiple studies have shown that the inherent ability of ECs to assemble into capillary-like structures can be capitalized on to generate a functional vasculature in 3D constructs in vivo.[10–13] For instance, we have shown that blood-derived ECFCs are capable of forming extensive functional vascular networks in vivo when combined with either smooth muscle cells[10] or MSCs[11] in a diverse range of natural hydrogels, including Matrigel, collagen gel and fibrin gel.[16] Others have proposed alternative sources of endothelial and perivascular cells,[12,13,34] but all of these studies fundamentally use the same approach: embedding vascular cells in natural hydrogels to achieve a 3D vascular architecture.[8,9] In the present study, we have demonstrated the suitability of a photocrosslinkable gelatin methacrylate (GelMA) hydrogel to support the human-progenitor-cell-based formation of 3D vascular networks. Using GelMA as the embedding scaffold, we have shown that 3D cocultures of human-blood-derived ECFCs and bone-marrow-derived MSCs generate extensive capillary-like networks in vitro (Figure 4d and Video 1, Supporting Information). These vascular structures contain distinct lumens that are formed by the fusion of ECFC intracellular vacuoles in a process of vascular morphogenesis (Figure 6). The process of vascular network formation is dependent on the presence of MSCs, which differentiate into perivascular cells occupying abluminal positions within the network (Figure 5a, 6d and Video 2, Supporting Information). Importantly, we have shown that the implantation of cell-laden GelMA hydrogels into immunodeficient mice results in the rapid formation of functional anastomoses between our engineered human vascular network and the mouse vasculature. Furthermore, we have also demonstrated that by altering the degree of methacrylation during the manufacture of GelMA, we are able to modify the extent of the vascular network formation, both in vitro and in vivo.

The use of polymeric hydrogels is now common practice in regenerative medicine research.[21,24,35,36] We recently proposed the use of GelMA to create cell-laden microtissue and microfluidic devices in an effort to overcome the shortcomings of other prevalent hydrogels, including poor mechanical properties, inadequate cell binding and viability, or the inability to control the hydrogel microarchitecture.[26] For example, native ECM molecules, such as collagen, are commonly used to create cell-laden hydrogels;[20,37] however, the ability to create lasting constructs is limited typically due to insufficient mechanical robustness.[16,19] Conversely, some synthetic hydrogels, such as polyethylene glycol (PEG)[30] or hyaluronic acid (HA),[23] have stronger mechanical properties, but inherently lack cell-responsive features, which limits their applicability in tissue engineering.[38] GelMA is a functionalized natural (gelatin) hydrogel, and therefore shares the advantages of both natural and synthetic hydrogels.[26] By simply modifying the degree of methacrylation, we have demonstrated that both the porosity and the degradability can be tuned to achieve a desirable mechanical robustness without compromising the cellular biocompatibility. These tunable mechanical properties have allowed us to fabricate GelMA hydrogels with slower in vivo contraction and degradation rates than collagen-type 1 gels, which are common limitations shared by the majority of natural hydrogels.[20] Also, GelMA hydrogels are based on gelatin, which is an inexpensive denatured collagen that can be derived from a variety of sources, making it a potentially attractive material for tissue engineering applications.

The presence of natural gelatin in GelMA should provide natural cell binding motifs and degradation sites, which, in principle, should facilitate cellular behavior.[26,29] We have demonstrated that GelMA hydrogels are permissive cellular environments, compatible with ECFCs and MSCs, and that the cellular behavior can be altered by modifying the degree of methacrylation. For instance, MSCs were able to spread and proliferate for a period of 6 d in three different GelMA monocultures, but the extent of spreading, organization and proliferation was dependent on the methacrylation degree, with the softer hydrogels being more permissive than the highly methacrylated ones. On the other hand, ECFCs were not able either to proliferate or spread in the GelMA monocultures, an observation that was true for all of the methacrylation degrees tested. However, this apparent inability was addressed in the presence of MSCs: co-cultures of ECFCs and MSCs in GelMA resulted in extensive, 3D capillary-like networks with an ECFC lining within these structures. Also,

the capacity of cellular assembly into vascular structures was affected by the methacrylation degree of the GelMA, with the softer hydrogels promoting more extensive networks. Collectively, our studies in vitro show the cellular suitability of GelMA, suggesting that the inherent biocompatibility of the natural gelatin is well preserved throughout the manufacturing process. In addition, our results indicate that, while GelMA provides a permissive environment for vascular morphogenesis, cell proliferation and organization into complex 3D structures is ultimately governed by heterotypic cellular interactions.

A critical aspect of vascular morphogenesis is the formation of functional lumens.[31] In vivo, the presence of human-specific lumen was unequivocally identified throughout the GelMA constructs at 7 d post-transplantation. The majority of these human ECFC-lined lumens contained murine erythrocytes, which indicates that functional connections with the host vasculature occurred. We have also demonstrated that the degree of methacrylation can be used to influence the extent of the vascular network formation and the average morphology of the engineered human blood vessels: a higher degree of methacrylation translates into constructs having a lower microvessel density and smaller lumens; these observations are in line with recent reports that correlate ECM mechanical properties and capillary cell shape and function.[39] Our results also illustrate specific details about the process of lumen formation within ECFC-lined capillary-like structures in vitro. This process involves early ECFC pinocytosis, which results in the formation of intracellular vesicles by day 3. The surface of these vesicles expressed a surface protein hCD31, suggesting that they were formed by invagination of the cell membrane.[31] Vacuoles were subsequently fused both intracellularly and extracellularly, resulting in hollowed lumen formation. To what extent the molecular machinery involved in vascular lumen formation in vitro resembles the formation of lumens in our in vivo model remains to be investigated further. In any case, GelMA hydrogel was found to be a permissive microenvironment that supports vascular morphogenesis and lumen formation.

4. Conclusions

In the present study, we have demonstrated the suitability of photocrosslinkable GelMA hydrogel to support human-progenitor-cell-based formation of 3D vascular networks in vitro and in vivo. Using GelMA as the embedding scaffold, we have shown that 3D co-cultures of human-blood-derived ECFCs and bone-marrow-derived MSCs generate extensive capillary-like networks that form functional anastomoses with the existing vasculature upon implantation into immunodeficient mice. We have also demonstrated that the physical properties of the GelMA are controllable through the variation of the degree of methacrylation, and that these variations can be used to tune the extent of the vascular network formation. Based on these data, we propose the use of GelMA hydrogels in future regenerative applications that require the formation of functional vascular beds, including the engineering of complex tissues and organs.

Experimental Section

Cell Culture: ECFCs and MSCs were isolated from human cord blood and bone marrow, as described previously.[11,40] The ECFCs were cultured on gelatin (1%)-coated tissue culture plates in endothelial basal medium (EBM-2; Lonza) supplemented with fetal bovine serum (FBS) (20%, Hyclone), SingleQuots (except for hydrocortisone) (Lonza), and 1× glutamine-penicillin-streptomycin (GPS) (Invitrogen). MSCs were cultured on uncoated plates using mesenchymal stem cell growth medium (MSCGM) (Lonza) with FBS (10%), 1× GPS and basic fibroblast growth factor (bFGF) (10 ng mL^{-1}, R&D System). ECFCs and MSCs between passages 6 and 9 were used for all of the experiments.

Retroviral Transduction of ECFCs: The ECFCs were genetically labeled with red-fluorescence proteins (DsRed) by retroviral infection with a pLVX-DsRed vector. Briefly, viruses were generated in human embryonic kidney (HEK) 293T cells with Virapower Lentiviral packaging mix and lipofectamine 2000 (Invitrogen). The ECFCs (1×10^6 cells at passage 1) were then incubated with 5 mL of virus stock for 6 h in the presence of protamine sulfate (12 µg mL^{-1}, Sigma–Aldrich). Puromycin-resistant transfected cells were selected with puromycin (2 µg mL^{-1}, Invitrogen) in regular culture medium. The DsRed-ECFCs were characterized by immunofluorescent staining and expressed the expected EC markers (Figure S11, Supporting Information).

Preparation of GelMA Hydrogels: GelMA was synthesized as described previously.[26] Briefly, type-A porcine skin gelatin (Sigma–Aldrich) was dissolved in Dulbecco's phosphate buffered saline (DPBS) (GIBCO) at 60 °C to make a uniform gelatin solution (10% (w/w)). Methacrylic anhydride (MA) (Sigma–Aldrich) was added to the gelatin solution at a rate of 0.5 mL min^{-1} under stirring conditions. Final concentrations of MA of 1, 5 and 10% (v/v) were used (referred to herein as 1M, 5M, and 10M GelMA). The mixture was allowed to react for 3 h at 50 °C. After a 5-times dilution with additional warm DPBS, the GelMA solution was dialyzed against deionized water using 12–14 kDa cut-off dialysis tubes (Spectrum Laboratories) for 7 d at 50 °C to remove unreacted MA and additional by-products. The dialyzed GelMA solutions were frozen at –80 °C, lyophilized, and stored at room temperature. Before use, a GelMA prepolymer solution was prepared by dissolving the freeze-dried GelMA (5 w/v% final) and the photoinitiator (Irgacure 2959) (0.5 w/v%, CIBA Chemicals) in DPBS at 80 °C. Photocrosslinking was achieved by exposing the GelMA prepolymer to 6.7 mW cm^{-2} UV light (360 –480 nm; using an OmniCure S2000 UV lamp (Lumen Dynamics)) for 20 s at room temperature.

Characterization of GelMA Hydrogels: The degree of methacrylation was quantified by using an NMR spectrometer (Varian INOVA) as previously described.[26] The compressive modulus of different hydrogels was calculated at a rate of 20% strain min^{-1} on a mechanical tester (Instron 5542) as previously described.[26] The enzymatic degradation properties of GelMA with different methacrylation degrees were determined in DPBS containing collagenase A (2 µg mL^{-1}, Roche Diagnostics) at 37 °C. The percentage of mass loss was determined at different time points by the ratio of the weight to the original weight. The nanostructures of the GelMA hydrogels were observed under a scanning electron microscope (SEM) (Supra55VP, Zeiss) at 15 kV as previously described.[41]

Encapsulation of ECFCs and MSCs in GelMA Hydrogels: Single-cell suspensions were centrifuged to form a pellet and suspended in the GelMA prepolymer solution at 37 °C. For the monoculture experiments, DsRed-ECFCs or MSCs were suspended at 2×10^6 cells mL^{-1} of GelMA. For the co-cultures, 1×10^6 DsRed-ECFCs and 1×10^6 MSCs were suspended in 1 mL of GelMA prepolymer solution. The cell-prepolymer mixture was dispensed as 100 µL drops (1 mm thick). Photocrosslinking was achieved by exposing the cell-prepolymer mixture to 6.7 mW cm^{-2} UV light (360 –480 nm) for 20 seconds. Thereafter, cell-laden hydrogels were cultured in an ECFC medium with 2% FBS instead of 20% FBS.

Encapsulated Cell Number: The cell laden hydrogels were digested with a 1 mg mL^{-1} collagenase-A solution for 20 min at 37 °C. The retrieved cells were counted using a hemocytometer. In the co-culture experiments, MSCs were prelabeled with a green fluorescence Celltracker, CMFDA (Invitrogen), for easier visualization. DsRed-labeled ECFCs were identified by red fluorescence.

In Vitro Capillary-Like Network Visualization: The cell laden hydrogels were whole-mounted on a glass-bottom dish (MatTek) and examined using a Leica SP5X MP inverted laser scanning confocal microscope. Serial optical sections were recorded, beginning at the bottom surface of the specimen, and the resultant stacks were rendered in three dimensions using Bitplane Imaris 7.1 software. The capillary-like networks were visualized by the red fluorescence of the DsRed-ECFCs. The total capillary-like length, the average length of capillary-like network, the number of capillary-like branches and the number of branches points were quantified on 3D projected confocal images using Image J software (NIH).

Immunofluorescence Staining: Intact, whole-mounted GelMA hydrogels were stained with anti-Ki67 (Millipore), anti-αSMA (Sigma–Aldrich), anti-sm-MHC (Biomedical Technologies) and anti-human-CD31 (DakoCytomation, Clone JC70A) antibodies. Briefly, cell-laden hydrogels were fixed in paraformaldehyde (4%) and permeabilized with Triton X-100 (0.5%) in DPBS for 25 min. The hydrogels were then blocked with bovine serum albumin (BSA) (1.5%, Sigma–Aldrich) in DPBS for 2 h, followed by overnight incubation with primary antibodies (1:100 dilution). After washing in DPBS three times, the hydrogels were incubated with Alexa Fluor 488-conjugated goat anti-mouse or anti-rabbit secondary antibodies (Invitrogen; 1:200 dilution) overnight. Finally, the hydrogels were stained with 4′,6-diamidino-2-phenylindole (DAPI) (Vector Laboratories), immersed in DPBS, and examined using a confocal microscope (Leica SP5X MP). 3D images were reconstructed by using Bitplane Imaris 7.1 software.

Mice: Six-week-old, male, athymic, nude (nu/nu) mice were purchased from Massachusetts General Hospital, MA. The mice were housed in compliance with the Children's Hospital guidelines, and all of the animal-related protocols were approved by the Institutional Animal Care and Use Committee.

In Vivo Degradation of GelMA: The GelMA hydrogels (200 μL) were polymerized as described previously and equilibrated overnight in DPBS. The next day, hydrogel constructs were surgically implanted into the subcutaneous space on the back of a six-week-old nu/nu mouse. Rat-tail type-1 collagen gel (3 mg mL^{-1} in DPBS; pH = 7.4; 200 μL; BD Biosciences) served as a control. Every mouse received a single hydrogel construct. After 7 and 28 d, the implants were harvested, imaged and weighed to determine the degradation degree of each hydrogel.

Blood Analysis: The hematologic parameters were determined for implant-bearing mice at 3, 7, 14, 21 and 28 d. Blood was collected by submandibular bleeding in 2,2′,2″,2‴-(ethane-1,2-diyldinitrilo)tetra-acetic acid (EDTA)-coated tubes (Sarstedt). The complete cell count (CBC) and the absolute differential white blood cell (WBC) count were obtained from whole blood using an automated complete blood count test (Department of Laboratory Medicine, Children's Hospital Boston).

In Vivo Vasculogenic Assay: The formation of vascular networks in vivo was evaluated using a xenograft model of transplantation into immunodeficient mice.[12,13] Briefly, 5×10^5 DsRed-ECFCs and 5×10^5 MSCs were embedded in 200 μL hydrogels and crosslinked as described. The cell laden hydrogels were incubated for 24 h in EGM-2 medium before implantation. The next day, the hydrogel constructs were surgically implanted into the subcutaneous spaces on the backs of six-week-old male nu/nu mice. Rat-tail type-1 collagen gel (3 mg mL^{-1} in DPBS; pH = 7.4) containing the same amount of cells served as a control. One construct was implanted per mouse. Each experimental condition was performed with 7 mice.

Histology and Immunohistochemistry: The mice were euthanized and the hydrogel implants were removed, fixed in buffered formalin (10%) overnight, embedded in paraffin, and sectioned. H&E staining was examined on 7 μm-thick sections for the presence of luminal structures containing red blood cells. For immunohistochemistry, 7 μm-thick sections were deparaffinized, and antigen retrieval was carried out by heating the sections in 2-amino-2-hydroxymethyl-propane-1,3-diol (Tris)-EDTA buffer (10 mM Tris-Base, 2 mM EDTA, 0.05% polyoxyethylene (20) sorbitan monolaurate (Tween-20), pH = 9.0). The sections were blocked for 30 min in blocking serum (5%) and incubated with primary antibodies for 1 h at room temperature. The following primary antibodies were used: mouse anti-human CD31 (for human microvessel detection; 1:50; DakoCytomation, Clone JC70A) and mouse anti-αSMA (for perivascular cell detection; 1:200; Sigma–Aldrich, Clone 1A4). For human-CD31 immunohistochemistry, horseradish peroxidase-conjugated mouse secondary antibodies (1:200; Vector Laboratories) and 3,3′-diaminobenzidine (Vector Laboratories) were used, followed by hematoxylin counterstaining and Permount mounting. For αSMA immunofluorescence, secondary antibody incubations were carried out for 1 h at room temperature using Alexa Fluor 488-conjugated anti-mouse secondary antibodies (1:200; Invitrogen). Rhodamine-labeled UEA-1 (1:100; Vector Laboratories) was used to detect human microvessels. All of the fluorescently stained sections were counterstained with DAPI.

Microvessel Density: The microvessels were quantified by evaluation of 10 randomly selected fields (under 40× magnification) of H&E stained sections taken from the middle part of the implants. The microvessels were identified as luminal structures containing red blood cells. The microvessel density was reported as the average number of erythrocyte-filled microvessels from the fields analyzed and expressed as vessels mm^{-2}. The values reported for each experimental condition are the mean values ± the standard deviation, obtained from seven individual mice. The percentages of human-specific microvessels and the luminal areas of the human microvessels were determined using the ImageJ software after human-CD31 immuno-histochemical staining (>50 vessels per section).

Statistical Analysis: Statistical analysis was performed using GraphPad Prism 5. All of the data are presented as the mean ± standard deviation of the mean. A comparison of values from different materials was carried out by one-way/two-way analysis of variance (ANOVA).

Supporting Information

Supporting Information is available from the Wiley Online Library or from the author.

Acknowledgements

Y.C.C and R.Z.L. contributed equally to this work. The histology was supported by the Specialized Research Pathology Cores, Longwood Facility of the Dana–Farber/Harvard Cancer Center (P30 CA06516). Automated CBCs were supported by the Core Laboratory of the Department of Laboratory Medicine at the Children's Hospital Boston. This work was partially supported by grants from the National Institute of Biomedical Imaging and Bioengineering (NIBIB) of the National Institutes of Health (EB009096 to J.M.-M) and NIH (HL092836, HL099073, DE019024 and EB012597 to A.K.; AR057837 and DE021468 to Y.Y.).

Received: July 20, 2011
Revised: October 6, 2011
Published online: February 21, 2012

[1] S. Levenberg, J. Rouwkema, M. Macdonald, E. S. Garfein, D. S. Kohane, D. C. Darland, R. Marini, C. A. van Blitterswijk, R. C. Mulligan, P. A. D'Amore, R. Langer, *Nat. Biotechnol.* **2005**, *23*, 879.
[2] R. Langer, J. P. Vacanti, *Science* **1993**, *260*, 920.
[3] R. K. Jain, P. Au, J. Tam, D. G. Duda, D. Fukumura, *Nat. Biotechnol.* **2005**, *23*, 821.
[4] J. M. Isner, T. Asahara, *J. Clinical Investigation* **1999**, *103*, 1231.
[5] J. M. Isner, A. Pieczek, R. Schainfeld, R. Blair, L. Haley, T. Asahara, K. Rosenfield, S. Razvi, K. Walsh, J. F. Symes, *Lancet* **1996**, *348*, 370.

[6] H. Lee, R. A. Cusick, F. Browne, T. Ho Kim, P. X. Ma, H. Utsunomiya, R. Langer, J. P. Vacanti, *Transplantation* **2002**, *73*, 1589.
[7] S. Rafii, D. Lyden, *Nat. Med.* **2003**, *9*, 702.
[8] N. Koike, D. Fukumura, O. Gralla, P. Au, J. S. Schechner, R. K. Jain, *Nature* **2004**, *428*, 138.
[9] J. S. Schechner, A. K. Nath, L. Zheng, M. S. Kluger, C. C. Hughes, M. R. Sierra-Honigmann, M. I. Lorber, G. Tellides, M. Kashgarian, A. L. Bothwell, J. S. Pober, *Proc. Natl. Acad. Sci. USA* **2000**, *97*, 9191.
[10] J. M. Melero-Martin, Z. A. Khan, A. Picard, X. Wu, S. Paruchuri, J. Bischoff, *Blood* **2007**, *109*, 4761.
[11] J. M. Melero-Martin, M. E. De Obaldia, S. Y. Kang, Z. A. Khan, L. Yuan, P. Oettgen, J. Bischoff, *Circulation Res.* **2008**, *103*, 194.
[12] P. Au, L. M. Daheron, D. G. Duda, K. S. Cohen, J. A. Tyrrell, R. M. Lanning, D. Fukumura, D. T. Scadden, R. K. Jain, *Blood* **2008**, *111*, 1302.
[13] D. O. Traktuev, D. N. Prater, S. Merfeld-Clauss, A. R. Sanjeevaiah, M. R. Saadatzadeh, M. Murphy, B. H. Johnstone, D. A. Ingram, K. L. March, *Circulation Res.* **2009**, *104*, 1410.
[14] R. Z. Lin, A. Dreyzin, K. Aamodt, A. C. Dudley, J. M. Melero-Martin, *Cell Transplantation* **2011**, *20*, 515.
[15] V. P. Shastri, *Adv. Mater.* **2009**, *21*, 3246.
[16] P. Allen, J. Melero-Martin, J. Bischoff, *J. Tissue Eng. Regenerative Med.* **2011**, *5*, e74.
[17] G. E. Davis, D. R. Senger, *Circulation Res.* **2005**, *97*, 1093.
[18] H. K. Kleinman, G. R. Martin, *Seminars Cancer Biol.* **2005**, *15*, 378.
[19] C. Helary, I. Bataille, A. Abed, C. Illoul, A. Anglo, L. Louedec, D. Letourneur, A. Meddahi-Pelle, M. M. Giraud-Guille, *Biomaterials* **2010**, *31*, 481.
[20] D. G. Wallace, J. Rosenblatt, *Adv. Drug Delivery Rev.* **2003**, *55*, 1631.
[21] A. S. Hoffman, *Adv. Drug Delivery Rev.* **2002**, *54*, 3.
[22] S. F. Badylak, T. W. Gilbert, *Seminars Immunology* **2008**, *20*, 109.
[23] D. Hanjaya-Putra, V. Bose, Y. I. Shen, J. Yee, S. Khetan, K. Fox-Talbot, C. Steenbergen, J. A. Burdick, S. Gerecht, *Blood* **2011**.
[24] B. V. Slaughter, S. S. Khurshid, O. Z. Fisher, A. Khademhosseini, N. A. Peppas, *Adv. Mater.* **2009**, *21*, 3307.
[25] J. Kohn, *Nat. Mater.* **2004**, *3*, 745.
[26] J. W. Nichol, S. T. Koshy, H. Bae, C. M. Hwang, S. Yamanlar, A. Khademhosseini, *Biomaterials* **2010**, *31*, 5536.
[27] K. Y. Lee, D. J. Mooney, *Chem. Rev.* **2001**, *101*, 1869.
[28] H. Qi, Y. Du, L. Wang, H. Kaji, H. Bae, A. Khademhosseini, *Adv. Mater.* **2010**, *22*, 5276.
[29] H. Aubin, J. W. Nichol, C. B. Hutson, H. Bae, A. L. Sieminski, D. M. Cropek, P. Akhyari, A. Khademhosseini, *Biomaterials* **2010**, *31*, 6941.
[30] J. J. Moon, J. E. Saik, R. A. Poche, J. E. Leslie-Barbick, S. H. Lee, A. A. Smith, M. E. Dickinson, J. L. West, *Biomaterials* **2010**, *31*, 3840.
[31] M. Kamei, W. B. Saunders, K. J. Bayless, L. Dye, G. E. Davis, B. M. Weinstein, *Nature* **2006**, *442*, 453.
[32] R. K. Jain, *Nat. Med.* **2003**, *9*, 685.
[33] E. C. Novosel, C. Kleinhans, P. J. Kluger, *Adv. Drug Delivery Rev.* **2011**, *63*, 300.
[34] X. Chen, A. S. Aledia, S. A. Popson, L. Him, C. C. Hughes, S. C. George, *Tissue Eng. Part A* **2010**, *16*, 585.
[35] A. Khademhosseini, R. Langer, *Biomaterials* **2007**, *28*, 5087.
[36] J. A. Burdick, G. D. Prestwich, *Adv. Mater.* **2011**, *23*, H41.
[37] C. B. Weinberg, E. Bell, *Science* **1986**, *231*, 397.
[38] M. P. Lutolf, J. A. Hubbell, *Nature Biotechnol.* **2005**, *23*, 47.
[39] A. Mammoto, K. M. Connor, T. Mammoto, C. W. Yung, D. Huh, C. M. Aderman, G. Mostoslavsky, L. E. Smith, D. E. Ingber, *Nature* **2009**, *457*, 1103.
[40] J. M. Melero-Martin, J. Bischoff, *Methods Enzymology* **2008**, *445*, 303.
[41] W. Xiao, J. He, J. W. Nichol, L. Wang, C. B. Hutson, B. Wang, Y. Du, H. Fan, A. Khademhosseini, *Acta Biomater.* **2011**, *7*, 2384.